Quantitative profiling of initiating ribosomes *in vivo*

Xiangwei Gao[1,5,6], Ji Wan[1,6], Botao Liu[2], Ming Ma[3], Ben Shen[3,4] & Shu-Bing Qian[1,2]

Cells have evolved exquisite mechanisms to fine-tune the rate of protein synthesis in response to stress. Systemic mapping of start-codon positions and precise measurement of the corresponding initiation rate would transform our understanding of translational control. Here we present quantitative translation initiation sequencing (QTI-seq), with which the initiating ribosomes can be profiled in real time at single-nucleotide resolution. Resultant initiation maps not only delineated variations of start-codon selection but also highlighted a dynamic range of initiation rates in response to nutrient starvation. The integrated data set provided unique insights into principles of alternative translation and mechanisms controlling different aspects of translation initiation. With RiboTag mice, QTI-seq permitted tissue-specific profiling of initiating ribosomes *in vivo*. Liver cell–specific ribosome profiling uncovered a robust translational reprogramming of the proteasome system in fasted mice. Our findings illuminated the prevalence and dynamic nature of translational regulation pivotal to physiological adaptation *in vivo*.

Translational regulation permits cells to respond swiftly to stress conditions via immediate and selective changes in protein expression levels[1–3]. Much of this translational control occurs at the initiation stage[4–7]. Although the importance of translation initiation has long been appreciated, direct measurement of the initiation rate on individual mRNAs has been difficult. Recent development of ribosome-profiling technology (Ribo-seq), based on deep sequencing of ribosome-protected mRNA fragments (RPFs), enables monitoring of ribosome dynamics with unprecedented resolution at the genome-wide scale[8,9]. The obtained snapshot of ribosome occupancy on the coding region has often been used to estimate relative changes of translation efficiency under different growth conditions. A caveat, however, exists because the average ribosome density on mRNAs is negatively influenced by the elongation speed[10,11]. Dynamic changes of initiation rates are thus masked by the varied elongation speed under different growth conditions. In addition, the average density of ribosome occupancy is not suitable to evaluate alternative translation events occurring on the same mRNA[12]. These constraints point to a need for a method capable of mapping start-codon selection and quantifying the rate of 80S ribosome assembly at individual translation initiation sites (TISs).

Much of our understanding of the basic mechanisms of translation initiation is limited to cells in culture. Investigating translational control at the organismal level remains a pressing and formidable challenge. The cellular heterogeneity of tissues and organs confounds our efforts to achieve cell type–specific genomic and proteomic interrogation. To monitor protein synthesis at the organismal level, one approach relies on tagged ribosomal proteins, such as hemagglutinin (HA)-tagged Rpl22 (ref. 13) or EGFP-fused Rpl10a (ref. 14). Following genetic targeting to specific cell populations, affinity purification allows isolation of polysome-bound mRNAs from specific cell types suitable for profiling assays. However, current methods do not allow tissue-specific profiling of initiating ribosomes, which bear more reliable information in evaluating translational control *in vivo*.

Here we present an approach called QTI-seq that allows comprehensive monitoring of translation initiation in cells and solid tissues. Together with the RNA-seq and Ribo-seq data sets acquired in parallel, the integrated ribosome-profiling data afford a holistic view of the translational landscape under different growth conditions.

RESULTS

QTI-seq captures initiating ribosomes in an unbiased manner

We previously developed global translation initiation sequencing (GTI-seq)[15], which capitalizes on the unique feature of lactimidomycin (LTM) that preferentially acts on the first 80S ribosome when its E site is empty[16]. However, LTM-mediated enrichment of initiating ribosomes requires an incubation of the cell at 37 °C to allow for the release of elongating ribosomes. This procedure, albeit essential for high-resolution mapping of TISs, may generate a number of artifacts. First, free ribosomes could start new rounds of initiation during the incubation period, resulting in an amplification of ribosome occupancy at the start codon (**Supplementary Fig. 1a**). Second, the amplified ribosome density is biased toward the upstream initiators, causing an unwanted 5′-end inflation of RPFs. When GTI-seq was applied to human HEK293 cells with amino acid deprivation, the LTM peaks at the annotated start codons (aTISs) showed few changes despite the pervasive reduction of ribosome occupancy on many transcripts

[1]Division of Nutritional Sciences, Cornell University, Ithaca, New York, USA. [2]Graduate Field of Genetics, Genomics & Development, Cornell University, Ithaca, New York, USA. [3]Department of Chemistry, The Scripps Research Institute, Jupiter, Florida, USA. [4]Molecular Therapeutics and Natural Products Library Initiative, The Scripps Research Institute, Jupiter, Florida, USA. [5]Present address: Institute of Environmental Medicine, Zhejiang University School of Medicine, Hangzhou, People's Republic of China. [6]These authors contributed equally to this work. Correspondence should be addressed to S.-B.Q. (sq38@cornell.edu).

RECEIVED 1 AUGUST; ACCEPTED 30 OCTOBER; PUBLISHED ONLINE 8 DECEMBER 2014; DOI:10.1038/NMETH.3208

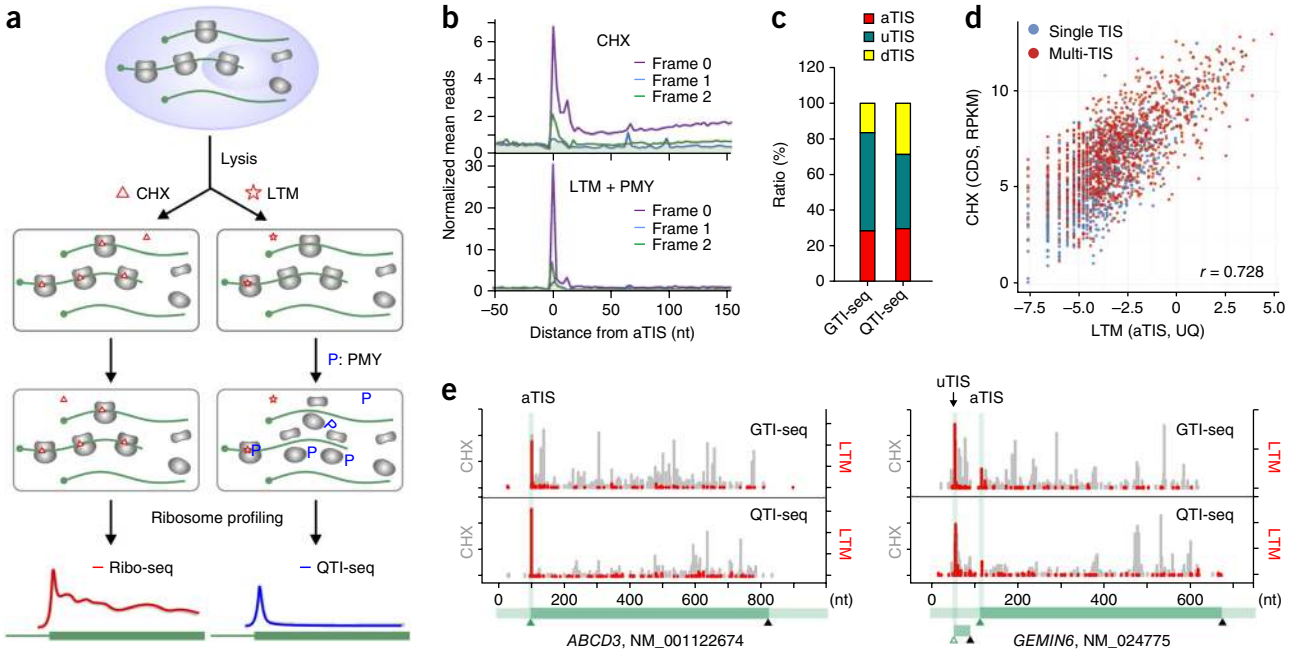

Figure 1 | QTI-seq captures real-time translation initiation events in a qualitative and quantitative manner. (**a**) Schematic of Ribo-seq (left) and QTI-seq (right) procedures. CHX, cycloheximide; LTM, lactimidomycin; PMY, puromycin. (**b**) Meta-gene analysis of CHX-associated ribosome density and LTM-associated ribosome density in HEK293 cells captured by QTI-seq. Normalized ribosome-protected mRNA fragment (RPF) reads are averaged across the entire transcriptome and aligned at the annotated start codon (aTIS). Different reading frames are separated and color coded. (**c**) Relative ratios of different types of TISs identified by GTI-seq or QTI-seq in HEK293 cells. uTIS, upstream TIS; dTIS, downstream TIS. (**d**) Correlation between LTM-associated aTIS density, normalized by upper quartile (UQ), and CHX-associated coding region (CDS) ribosome occupancy, normalized by reads per kilobase per million reads (RPKM). Genes with a single aTIS or multiple TISs are shown as blue and red dots, respectively. (**e**) Examples of single-TIS (*ABCD3*) and multiple-TIS (*GEMIN6*) genes revealed by GTI-seq (top) and QTI-seq (bottom). The *y*-axis scales are identical. The corresponding gene structure is shown below the *x* axis.

(**Supplementary Fig. 1b**). As a result, virtually no correlation was found between the differences of LTM-captured aTIS density and the ribosome occupancy on the coding region (CDS) (**Supplementary Fig. 1c**). The lack of quantitative features in GTI-seq largely hampers comparative interrogation of translational regulation.

To circumvent this limitation, we set out to devise QTI-seq to preserve the small population of initiating ribosomes with minimal perturbation. Following extensive optimization, we implemented three steps to achieve this goal: (i) rapidly break down cells using lysing matrix D, which has a minimal effect on ribosome stability; (ii) specifically freeze the initiating ribosomes by treating cell lysates with LTM; and (iii) effectively deplete the elongating ribosomes by introducing another translation inhibitor, puromycin (PMY) (**Fig. 1a**). PMY does not affect translation initiation and has been used previously to enrich the initiating ribosomes[17]. Acting as a tRNA analog, PMY releases the nascent chain and dissociates the ribosome into separate subunits[18]. In the presence of elongation inhibitors such as cycloheximide (CHX), however, addition of PMY catalyzes puromycylation of the nascent chain without triggering ribosome dissociation[19]. The same feature holds true for cell-free samples as the presence of CHX completely prevented PMY-induced polysome disassembly (**Supplementary Fig. 2**). Because LTM uses a similar mechanism to that of CHX but selectively acts on the first 80S ribosome[16], we reasoned that sequential treatment with LTM and PMY would dissociate the elongating ribosomes but leave the initiating ribosomes insensitive to PMY (**Fig. 1a**). Indeed, PMY addition in the presence of LTM resulted in polysome disassembly with a corresponding increase of the monosome (**Supplementary Fig. 2**). To examine whether the increased monosome contained the preserved initiating ribosomes, we purified RPFs followed by deep sequencing. Metagene analysis revealed that the LTM-associated RPF reads were highly enriched at the aTIS codon (**Fig. 1b**). Additionally, the aTIS ribosome density captured by LTM was highly reproducible (**Supplementary Fig. 3**).

Because QTI-seq captured a small population of initiating ribosomes without 5′-end RPF inflation, QTI-seq identified fewer total TISs than GTI-seq in HEK293 cells (5,099 vs. 13,915), especially the upstream TIS codons (uTISs) (**Fig. 1c**). Consistent with previous reports[15,20], codon composition analysis revealed that more than half the TISs used a non-AUG sequence as the translation initiator (**Supplementary Fig. 4**). The associated LTM peak height at the aTISs showed a strong correlation with the average ribosome occupancy along the corresponding CDS (r = 0.728; **Fig. 1d**). In addition to this quantitative feature, QTI-seq retained the high precision in mapping TIS positions at a single-nucleotide resolution. For instance, a prominent LTM peak was located exactly at the annotated start codon of *ABCD3*; an out-of-frame uTIS was uncovered in *GEMIN6* (**Fig. 1e**). QTI-seq thus offers a promising approach to exploring real-time translation initiation in a qualitative and quantitative manner.

Quantitative TIS profile in response to starvation

We next applied QTI-seq to HEK293 cells with amino acid deprivation (**Supplementary Fig. 5**). Total cellular RNA was also

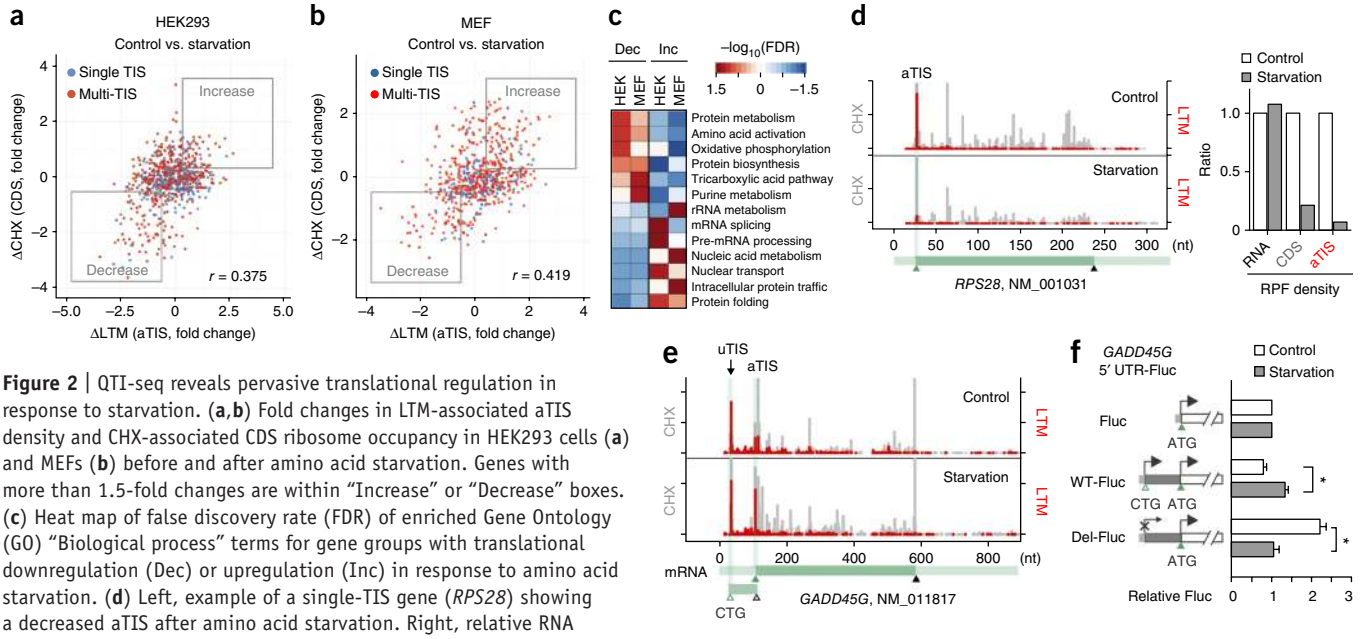

Figure 2 | QTI-seq reveals pervasive translational regulation in response to starvation. (**a**,**b**) Fold changes in LTM-associated aTIS density and CHX-associated CDS ribosome occupancy in HEK293 cells (**a**) and MEFs (**b**) before and after amino acid starvation. Genes with more than 1.5-fold changes are within "Increase" or "Decrease" boxes. (**c**) Heat map of false discovery rate (FDR) of enriched Gene Ontology (GO) "Biological process" terms for gene groups with translational downregulation (Dec) or upregulation (Inc) in response to amino acid starvation. (**d**) Left, example of a single-TIS gene (*RPS28*) showing a decreased aTIS after amino acid starvation. Right, relative RNA abundance, CDS ribosome occupancy and aTIS ribosome density of *RPS28*. (**e**) Example of a multiple-TIS gene (*GADD45G*) showing an increased aTIS fraction after amino acid starvation. (**f**) Experimental validation of translational control of GADD45G by a firefly luciferase (Fluc) reporter bearing the 5′ UTR of *GADD45G* with (WT) or without the uTIS codon CTG (Del). Data are mean ± s.e.m.; $n = 3$ biological replicates; $^*P < 0.05$ by Student's t-test.

collected in parallel for RNA-seq to quantify mRNA abundance. In response to starvation, the changes in the initiation rates showed positive correlation with the differences of ribosome occupancy on the corresponding CDS ($r = 0.375$; **Fig. 2a**). The same observation held for a mouse embryonic fibroblast (MEF) cell line subjected to starvation ($r = 0.419$; **Fig. 2b**). The imperfect correlation was partially due to reduced elongation speed under nutrient starvation that potentially increases the CDS ribosome occupancy (**Supplementary Fig. 6**). From the comprehensive data sets acquired from QTI-seq and Ribo-seq, we identified a large number of transcripts that underwent twofold changes upon starvation (1,073 in HEK293 cells and 820 in MEFs; **Supplementary Tables 1** and **2**). Among the genes showing repressed translation, many of them are involved in protein biosynthesis and metabolism (**Fig. 2c**). As a typical example, the gene encoding ribosomal protein RPS28 showed a nearly fivefold decrease in ribosome occupancy on the CDS in response to starvation (**Fig. 2d**). Remarkably, QTI-seq displayed a decrease greater than 14-fold in the ribosome density at the start codon of *RPS28*. Without the negative influence imposed by elongation speed variation, QTI-seq sets itself apart from previous methods by reporting true measures of initiation rates.

QTI-seq also captured a considerable number of genes whose transcripts experienced increased initiation in response to starvation (638 in HEK293 cells and 515 in MEFs). Interestingly, many of these genes are involved in protein folding and nuclear transport (**Fig. 2c**). Using a firefly luciferase (Fluc) reporter containing the 5′ UTR, we validated the translational upregulation of nucleoporin-encoding gene *NUP88* (**Supplementary Fig. 7**). It is noteworthy that many starvation-responsive genes contain multiple TISs (1,286 in HEK293 cells and 1,343 in MEFs), which suggests a regulatory role for alternative TISs in translational control[21]. To demonstrate the influence of alternative translation on the aTIS initiation, we selected genes with multiple TISs and computed the ribosome density at the aTIS codon relative to the total TIS density on the same transcript (**Supplementary Fig. 8**). This analysis uncovered many genes whose translational regulation is indiscernible by simple comparison of ribosome density changes at either CDSs or aTISs. A total of 428 genes in HEK293 cells and 212 genes in MEFs demonstrated an altered aTIS-to-TIS ratio upon amino acid deprivation (false discovery rate <0.05). This strategy uncovered several stress-responsive genes whose transcripts contain previously uncharacterized TISs. For instance, *GADD45G* bears a CUG start codon in the 5′ UTR (**Fig. 2e**). Fluc reporter assays confirmed the critical role of 5′ UTR in the starvation-induced upregulation of *GADD45G* (**Fig. 2f**). In particular, deleting the CUG codon was sufficient to prevent the starvation responsiveness.

Programmatic TIS regulation in response to starvation

Many upstream open reading frames are believed to exert negative effects on the main open reading frame translation, presumably by capturing the scanning ribosome[12,22]. It is thus not surprising to find that a large number of multiple-TIS–containing genes showed increased aTIS initiation when uTIS initiation was repressed under starvation. However, a handful of transcripts exhibited decreased aTIS fraction despite the presence of alternative TISs (**Supplementary Fig. 8**). To identify possible factors governing differential regulation of alternative TISs, we surveyed for consensus sequence motifs in gene groups that respond differently to starvation. Among transcripts with increased aTIS initiation upon starvation, the Kozak consensus motif was prominent (**Supplementary Fig. 9a**). For transcripts with increased uTISs, an evident purine-rich sequence context emerged above the background (**Supplementary Fig. 9b**). This finding is reminiscent of the polypurine (A)-rich sequences found in many evolutionarily

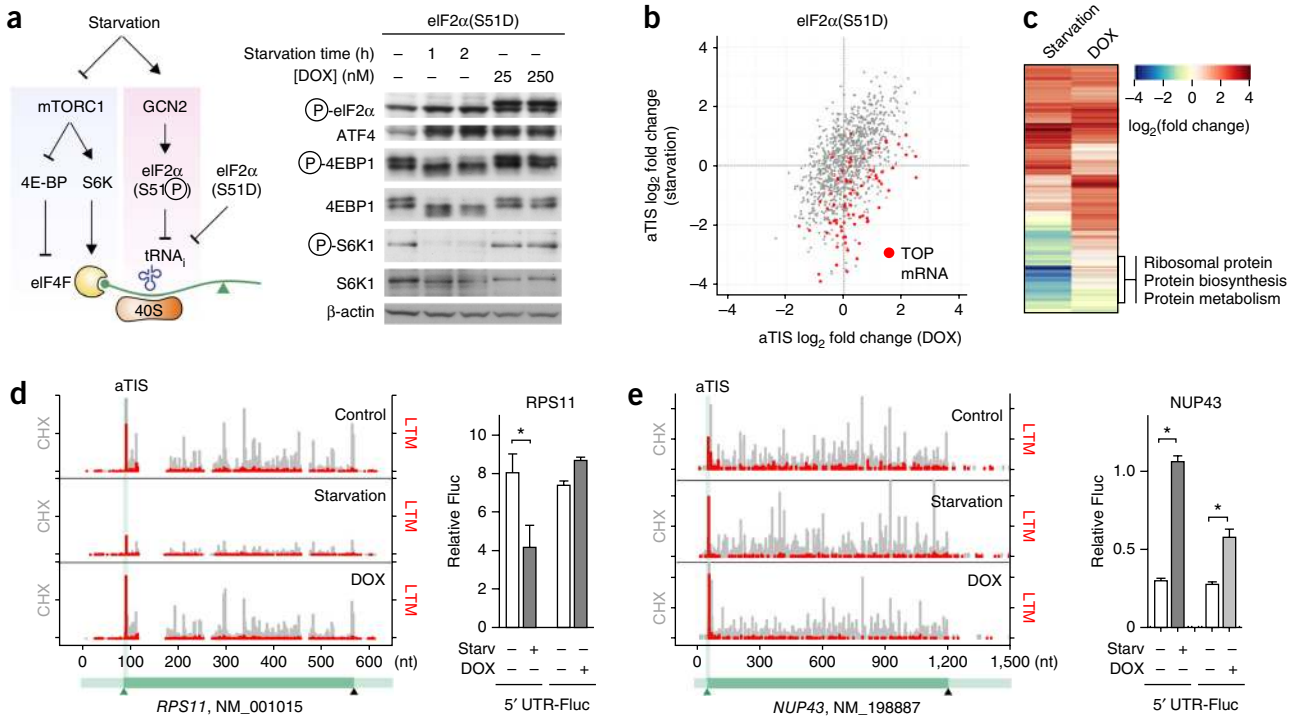

Figure 3 | Distinct role of eIF2α phosphorylation in translational response to starvation. (**a**) Left, schematic of mTORC1 signaling and eIF2α phosphorylation response. Right, immunoblotting results of eIF2α(S51D) mutant cells with either amino acid starvation or doxycycline (DOX)-induced eIF2α(S51D) expression. (**b**) Fold changes in LTM-associated aTIS density in eIF2α(S51D) mutant cells between amino acid starvation and DOX-induced eIF2α(S51D) expression. Terminal oligopyrimidine (TOP) mRNAs are shown as red dots. (**c**) Heat map of fold change of enriched GO terms ("Biological process") for gene groups with translational downregulation (blue) or upregulation (red) in response to amino acid starvation or DOX-induced eIF2α(S51D) expression. (**d**) Left, example of a gene (*RPS11*) showing translational repression in response to amino acid starvation but not DOX-induced eIF2α(S51D) expression. Right, validation of RPS11 translational control by a Fluc reporter bearing the 5′ UTR of *RPS11*. (**e**) Left, example of a gene (*NUP43*) showing translational upregulation in response to either amino acid starvation or DOX-induced eIF2α(S51D) expression. Right, validation of NUP43 translational control by a Fluc reporter bearing the 5′ UTR of *NUP43*. Data in **d**,**e** are mean ± s.e.m.; $n = 3$ biological replicates; $^*P < 0.01$ by Student's *t*-test.

conserved internal ribosome entry sites[23,24]. Alternatively, the purine-rich sequence may act in a manner opposite to the 5′ terminal oligopyrimidine (TOP) tract, whose translation is highly sensitive to the mTORC1 signaling pathway[25,26].

TIS regulation pathways in response to starvation

Amino acid deprivation suppresses global protein synthesis by inhibiting the mTORC1 signaling pathway and activating GCN2 kinases[27]. Whereas the former regulates cap recognition, the latter controls the ternary complex formation (**Fig. 3a**). It is unclear whether these distinct signaling pathways have overlapping or unique contributions to the translational regulation. We took advantage of a HEK293 cell line harboring an inducible phosphor-mimetic allele of eIF2α in which serine 51 was mutated to an aspartic acid (S51D)[28]. Expression of this mutant upon doxycycline (DOX) addition led to translational attenuation as well as an evident induction of ATF4 (**Fig. 3a** and **Supplementary Fig. 10a**). Unlike amino acid deprivation, however, eIF2α(S51D) expression had little effect on mTORC1 signaling (**Fig. 3a**). Therefore, the direct contribution of eIF2α phosphorylation to translational reprogramming can be dissected without pleiotropic effects caused by nutrient deprivation.

We applied QTI-seq to HEK293/eIF2α(S51D) cells with or without DOX treatment, together with RNA-seq and Ribo-seq. Similarly to amino acid starvation, eIF2α(S51D) expression resulted in evident differences for the LTM-associated aTIS ribosome density captured by QTI-seq (**Supplementary Fig. 10b** and **Supplementary Table 3**). A comparative analysis of the aTIS profiles between these two conditions revealed a partially overlapping gene pattern (**Fig. 3b**). Interestingly, the majority of overlapping genes were translationally upregulated with increased aTIS ribosome density. For those mRNAs undergoing translational repression under starvation, very few were affected in the presence of eIF2α(S51D), with the most notable gene group as TOP mRNAs (**Fig. 3b**). Clustering of the transcripts with changed aTIS ribosome density further confirmed the dichotomy of regulation between eIF2α(S51D) expression and starvation (**Fig. 3c**). In general, the transcripts commonly affected under both conditions were translationally upregulated and span diverse functions, whereas the starvation-sensitive mRNA subsets were translationally repressed and enriched in functions highly relevant to ribosome biogenesis. These results indicate that, in response to amino acid starvation, reduced mTORC1 signaling is more responsible for the suppression of TOP mRNA translation. In contrast, eIF2α phosphorylation contributes mainly to the selective upregulation of a subset of transcripts.

To confirm the differential regulation of translation initiation controlled by distinct upstream signaling pathways, we chose two genes for experimental validation. The gene encoding ribosomal protein RPS11 contains a typical TOP sequence on its 5′ UTR.

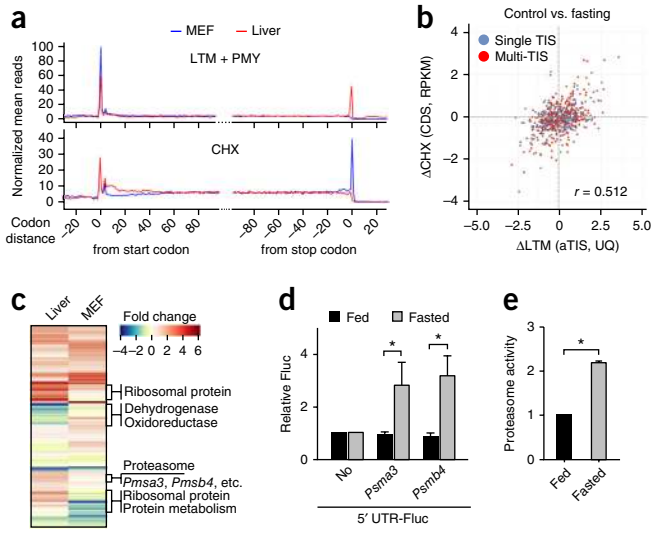

Figure 4 | Liver-specific QTI-seq reveals translational reprogramming in response to fasting. (**a**) Metagene analysis of LTM-associated ribosome density (top) or CHX-associated ribosome density (bottom) in MEFs and liver cells. Normalized RPF reads are averaged across the entire transcriptome and aligned at the annotated start codons and stop codons. (**b**) Fold changes in LTM-associated aTIS density and CHX-associated CDS ribosome occupancy in mouse liver cells with and without fasting. (**c**) Heat map of fold changes for gene groups with translational downregulation (blue) or upregulation (red) in liver cells of fasted mice or starved MEFs. (**d**) Reporter assay using an *in vitro* translation system reprogrammed from mouse liver lysates with or without fasting. The relative translation efficiency of a synthesized Fluc mRNA containing 5′ UTRs of *Psma3* or *Psmb4* is shown along with a no–5′ UTR condition. (**e**) Chymotrypsin activity of liver homogenates from mice 8–12 weeks old that were either fed or food deprived overnight, measured by Proteasome-Glo. Data in **d**,**e** are mean ± s.e.m.; $n = 3$ biological replicates; $^*P < 0.01$ by Student's t-test.

Amino acid starvation led to an approximately threefold decrease of the aTIS ribosome density (**Fig. 3d**). However, the translation of RPS11 exhibited little change in response to DOX-induced eIF2a(S51D) expression. The Fluc reporter bearing the *RPS11* 5′ UTR behaved exactly like the endogenous RPS11 in transfected cells (**Fig. 3d**). Amino acid starvation, but not eIF2a(S51D) expression, caused a significant reduction of Fluc expression. Unlike *RPS11*, the nucleoporin gene *NUP43* exhibited a translational upregulation after starvation or eIF2a(S51D) expression as evidenced by a more-than-threefold increase for its aTIS ribosome density (**Fig. 3e**). In agreement with the QTI-seq data, the Fluc reporter fused with the 5′ UTR of *NUP43* showed a consistent increase of translation in response to both conditions (**Fig. 3e**). These results strongly favor the hypothesis that distinct upstream signaling pathways act on different aspects of translation initiation, resulting in a coordinated translational reprogramming to achieve cellular adaptation.

Tissue-specific QTI-seq in liver cells

Having elucidated translational regulation from cells in culture, we reasoned that the principle of QTI-seq is applicable to solid tissues because it directly captures initiating ribosomes from lysates. To achieve cell type–specific ribosome profiling, we made use of the available RiboTag mouse, which carries a 'floxed' *Rpl22*^{HA} allele[13]. As a pilot study, we crossed the RiboTag mouse with a mouse expressing liver cell–specific Cre recombinase under the control of albumin promoter (Alb-Cre) (**Supplementary Fig. 11a**). The tissue specificity of Rpl22^{HA} incorporation into the ribosome was confirmed by anti-HA immunoprecipitation of polysome fractions (**Supplementary Fig. 11b**,**c**). In particular, the hepatocyte-specific transcripts were highly enriched in the tagged ribosome-associated mRNAs (**Supplementary Fig. 11d**). Following homogenization of liver tissues in the presence of LTM, PMY treatment led to efficient disassociation of the nonimmobilized ribosomes (**Supplementary Fig. 12a**). The LTM-preserved ribosome complexes bearing Rpl22^{HA} were enriched by anti-HA immunoprecipitation after RNase I digestion. Metagene analysis revealed an elevated ribosome density at the annotated start codon, a result suggesting that QTI-seq worked equally well in solid tissue samples (**Fig. 4a**). There were fewer TISs identified from liver cells than from MEFs (5,796 vs. 1,770), but they had a similar codon composition of TIS types (**Supplementary Fig. 13**). In addition, there was considerable overlap for the identified TISs between the two samples, and the overlap was further increased when we considered only the aTISs (**Supplementary Fig. 14**). The nonoverlapping TISs could be classified into differential aTISs and cell type–specific alternative TISs. For instance, the gene encoding hydroxyacyl-CoA dehydrogenase (HADH) showed a clear LTM peak at the aTIS in both liver and MEF samples (**Supplementary Fig. 15**). However, an in-frame downstream TIS was evident in the liver sample but vaguely present in the MEF sample. It is likely that liver cells can give rise to different isoforms of HADH enzyme.

Liver-specific TIS profile in response to fasting

The successful application of QTI-seq in mouse liver offers a unique opportunity to explore the translational response to a fasting condition at the organismal level. To this end, liver-specific RiboTag mice were subject to overnight fasting followed by RNA-seq, Ribo-seq and QTI-seq. Food deprivation resulted in large disassembly of polysomes in liver tissues (**Supplementary Fig. 12a**). Consistently, liver-specific QTI-seq uncovered extensive changes of ribosome density at the aTISs (**Supplementary Fig. 12b** and **Supplementary Table 4**). Supporting the quantitative feature of liver-specific QTI-seq, the changes of aTIS ribosome density in response to fasting correlated well with the differences of CDS ribosome occupancy ($r = 0.512$; **Fig. 4b**). Interestingly, overnight fasting elicited distinct translational responses in liver cells when compared to MEFs under starvation (**Fig. 4c**). Although MEFs showed prominent repression of ribosome biogenesis in response to starvation, this negative translational response was no longer obvious in liver cells after overnight fasting. In fact, some ribosomal protein genes underwent translational upregulation in fasted liver. This observation suggests that, contrary to the widely accepted notion, global inhibition of the translation machinery is a transient response upon acute nutrient deprivation. Under prolonged fasting conditions, a continuous supply of ribosomal proteins is likely needed for selective protein synthesis.

Many of the transcripts showing higher aTIS ribosome density encode components of the protein degradation pathway, in particular the proteasome system (**Fig. 4c**). This is consistent with the finding that the ubiquitin-proteasome system not only helps to remove misfolded or damaged proteins[29] but also contributes to intracellular amino acid recycling during nutrient deprivation[30].

Our results—for the first time, to our knowledge—demonstrate a translational mechanism that promotes the proteasome activity in response to prolonged fasting. To obtain direct evidence for translational control of the proteasome system, we cloned the 5′ UTR of several proteasome genes and fused them to the Fluc reporter. We established a reconstituted translation system programmed from the liver homogenates to mimic the *in vivo* translation environment. Using equal amounts of synthesized mRNAs, we found that the presence of 5′ UTR of *Psma3* or *Psmb4* resulted in a greater-than-threefold increase of Fluc activity in liver cells obtained from fasted mice but not in liver cells from normally fed mice (**Fig. 4d**). To ascertain the functional consequence of this translational switch in response to fasting, we directly measured the proteasome activity in liver homogenates using Proteasome-Glo. Overnight fasting resulted in a more-than-twofold increase in the proteasome chymotrypsin activity (**Fig. 4e**). Our results indicate a coordinated regulation between protein synthesis and degradation, which provides an elegant mechanism for cells and tissues to achieve metabolic homeostasis under nutrient deprivation.

DISCUSSION

Translation initiation is a crucial point of regulation in eukaryotic gene expression, allowing cells to adapt rapidly to changing environmental conditions[4–7]. The significance of translation initiation is further substantiated by the existence of alternative translation that utilizes one or more potential TISs in addition to the main start codon[12]. The ability to monitor quantitatively the engagement of 80S ribosomes at the individual TIS would provide an effective means to evaluate start codon selection and to uncover fundamental principles underlying translational regulation. Compared to GTI-seq, which we developed previously[15], QTI-seq represents a conceptually distinct approach that permits quantitative profiling of initiating ribosomes in samples from cells in culture and solid tissues.

The applicability of QTI-seq to solid tissues has the potential to greatly advance our understanding of the basic mechanisms of translation initiation from cellular to organismal levels. Using RiboTag mice, we demonstrated liver cell–specific profiling of initiating ribosomes. This can serve as a prototype for tissue-specific ribosome profiling using other techniques such as bacTRAP[14]. QTI-seq revealed that after overnight fasting, liver cells had a pattern of translational response distinct from that of MEFs under acute starvation, as follows. First, the global reduction of TOP mRNA translation was no longer evident, which suggests that a continuous supply of ribosomal proteins is needed for selective protein synthesis. Second, QTI-seq uncovered a potent translational reprogramming for the proteasome system. The ubiquitin-proteasome system targets many proteins for degradation, and the lethality of proteasome inhibition has been attributed to amino acid scarcity[31]. It therefore makes intuitive sense that the upregulation of the proteasome system is essential for cell survival so as to continuously supply amino acids. It will be of much interest to demonstrate this phenomenon in other types of tissues, such as skeletal muscle, in response to fasting.

METHODS

Methods and any associated references are available in the online version of the paper.

Accession codes. NCBI Sequence Read Archive: raw sequence data have been deposited under accession SRA160745.

Note: Any Supplementary Information and Source Data files are available in the online version of the paper.

ACKNOWLEDGMENTS

We thank the Qian lab members for helpful discussion; J. Parker and R. Weiss for critical reading of the manuscript; P. Walter (University of California at San Francisco) for the eIF2α(S51D) cell line; and Cornell University Life Sciences Core Laboratory Center for performing deep sequencing. This work was supported by grants to B.S. from the US National Institutes of Health (NIH CA106150) and to S.-B.Q. from the NIH (DP2 OD006449, R01AG042400), Ellison Medical Foundation (AG-NS-0605-09) and US Department of Defense (W81XWH-14-1-0068).

AUTHOR CONTRIBUTIONS

X.G. and S.-B.Q. conceived of the original idea. X.G. designed experimental approaches and performed the experiments. J.W. analyzed the data. B.L. assisted data interpretation. M.M. and B.S. synthesized LTM. S.-B.Q. wrote the paper.

COMPETING FINANCIAL INTERESTS

The authors declare no competing financial interests.

1. Aitken, C.E. & Lorsch, J.R. A mechanistic overview of translation initiation in eukaryotes. *Nat. Struct. Mol. Biol.* **19**, 568–576 (2012).
2. Gray, N.K. & Wickens, M. Control of translation initiation in animals. *Annu. Rev. Cell Dev. Biol.* **14**, 399–458 (1998).
3. Gebauer, F. & Hentze, M.W. Molecular mechanisms of translational control. *Nat. Rev. Mol. Cell Biol.* **5**, 827–835 (2004).
4. Sonenberg, N. & Hinnebusch, A.G. Regulation of translation initiation in eukaryotes: mechanisms and biological targets. *Cell* **136**, 731–745 (2009).
5. Spriggs, K.A., Bushell, M. & Willis, A.E. Translational regulation of gene expression during conditions of cell stress. *Mol. Cell* **40**, 228–237 (2010).
6. Liu, B. & Qian, S.B. Translational reprogramming in cellular stress response. *Wiley Interdiscip. Rev. RNA* **5**, 301–315 (2014).
7. Jackson, R.J., Hellen, C.U. & Pestova, T.V. The mechanism of eukaryotic translation initiation and principles of its regulation. *Nat. Rev. Mol. Cell Biol.* **11**, 113–127 (2010).
8. Ingolia, N.T., Ghaemmaghami, S., Newman, J.R. & Weissman, J.S. Genome-wide analysis *in vivo* of translation with nucleotide resolution using ribosome profiling. *Science* **324**, 218–223 (2009).
9. Ingolia, N.T. Ribosome profiling: new views of translation, from single codons to genome scale. *Nat. Rev. Genet.* **15**, 205–213 (2014).
10. Plotkin, J.B. & Kudla, G. Synonymous but not the same: the causes and consequences of codon bias. *Nat. Rev. Genet.* **12**, 32–42 (2011).
11. Shah, P., Ding, Y., Niemczyk, M., Kudla, G. & Plotkin, J.B. Rate-limiting steps in yeast protein translation. *Cell* **153**, 1589–1601 (2013).
12. Morris, D.R. & Geballe, A.P. Upstream open reading frames as regulators of mRNA translation. *Mol. Cell. Biol.* **20**, 8635–8642 (2000).
13. Sanz, E. *et al.* Cell-type-specific isolation of ribosome-associated mRNA from complex tissues. *Proc. Natl. Acad. Sci. USA* **106**, 13939–13944 (2009).
14. Heiman, M. *et al.* A translational profiling approach for the molecular characterization of CNS cell types. *Cell* **135**, 738–748 (2008).
15. Lee, S., Liu, B., Huang, S.X., Shen, B. & Qian, S.B. Global mapping of translation initiation sites in mammalian cells at single-nucleotide resolution. *Proc. Natl. Acad. Sci. USA* **109**, E2424–E2432 (2012).
16. Schneider-Poetsch, T. *et al.* Inhibition of eukaryotic translation elongation by cycloheximide and lactimidomycin. *Nat. Chem. Biol.* **6**, 209–217 (2010).
17. Fritsch, C. *et al.* Genome-wide search for novel human uORFs and N-terminal protein extensions using ribosomal footprinting. *Genome Res.* **22**, 2208–2218 (2012).
18. Blobel, G. & Sabatini, D. Dissociation of mammalian polyribosomes into subunits by puromycin. *Proc. Natl. Acad. Sci. USA* **68**, 390–394 (1971).
19. David, A. *et al.* Nuclear translation visualized by ribosome-bound nascent chain puromycylation. *J. Cell Biol.* **197**, 45–57 (2012).
20. Ingolia, N.T., Lareau, L.F. & Weissman, J.S. Ribosome profiling of mouse embryonic stem cells reveals the complexity and dynamics of mammalian proteomes. *Cell* **147**, 789–802 (2011).

21. Calvo, S.E., Pagliarini, D.J. & Mootha, V.K. Upstream open reading frames cause widespread reduction of protein expression and are polymorphic among humans. *Proc. Natl. Acad. Sci. USA* **106**, 7507–7512 (2009).
22. Kozak, M. Pushing the limits of the scanning mechanism for initiation of translation. *Gene* **299**, 1–34 (2002).
23. Dorokhov, Y.L. *et al.* Polypurine (A)-rich sequences promote cross-kingdom conservation of internal ribosome entry. *Proc. Natl. Acad. Sci. USA* **99**, 5301–5306 (2002).
24. Gilbert, W.V., Zhou, K., Butler, T.K. & Doudna, J.A. Cap-independent translation is required for starvation-induced differentiation in yeast. *Science* **317**, 1224–1227 (2007).
25. Meyuhas, O. Synthesis of the translational apparatus is regulated at the translational level. *Eur. J. Biochem.* **267**, 6321–6330 (2000).
26. Hamilton, T.L., Stoneley, M., Spriggs, K.A. & Bushell, M. TOPs and their regulation. *Biochem. Soc. Trans.* **34**, 12–16 (2006).
27. Hinnebusch, A.G. Translational regulation of GCN4 and the general amino acid control of yeast. *Annu. Rev. Microbiol.* **59**, 407–450 (2005).
28. Sidrauski, C. *et al.* Pharmacological brake-release of mRNA translation enhances cognitive memory. *Elife* **2**, e00498 (2013).
29. Sherman, M.Y. & Goldberg, A.L. Cellular defenses against unfolded proteins: a cell biologist thinks about neurodegenerative diseases. *Neuron* **29**, 15–32 (2001).
30. Vabulas, R.M. & Hartl, F.U. Protein synthesis upon acute nutrient restriction relies on proteasome function. *Science* **310**, 1960–1963 (2005).
31. Suraweera, A., Munch, C., Hanssum, A. & Bertolotti, A. Failure of amino acid homeostasis causes cell death following proteasome inhibition. *Mol. Cell* **48**, 242–253 (2012).

ONLINE METHODS

Cells and reagents. HEK293, HEK293Trex, and MEF cells were maintained in Dulbecco's modified Eagle's medium (DMEM) with 10% fetal bovine serum (FBS). Cycloheximide (CHX) and puromycin were purchased from Sigma. Plasmids transfection was performed using Lipofectamine 2000 (Invitrogen) following the manufacturer's instructions. The cell lines were not tested for mycoplasma contamination or authenticated for these experiments.

Animal treatment. The RiboTag mice and the Alb-Cre mice were purchased from Jackson Laboratory. Mice were housed in a temperature- and humidity-controlled facility with a 12-h light-dark cycle. The RiboTag mouse was bred to the Alb-Cre mouse line to obtain *Rpl22*^{HA}-expressing homozygous mice. Mice at the age of 8–12 weeks were subjected to overnight fasting. All animal procedures were approved by Cornell IACUC (#2008-0167).

Reproducibility. The experiments were not randomized. The investigators were not blinded to allocation during experiments and outcome assessment. No sample-size estimates were performed to ensure adequate power to detect a prespecified effect size.

Preparation of cell lysates. For cell lysates, two 10-cm dishes of cells were harvested in 400 µL ice-cold polysome buffer (10 mM HEPES, pH 7.4, 100 mM KCl, 5 mM $MgCl_2$) containing CHX (100 µg/mL) or lactimidomycin (LTM; 5 µM). Cells were then disrupted by vortexing using lysing matrix D (Fisher) six times for 20 s, followed by a 40-s interval on ice. After centrifugation at 4 °C and 12,000*g* for 10 min, the supernatant was saved for puromycin treatment. For liver homogenates, male RiboTag/Alb-Cre mice with or without overnight fasting were sacrificed by decapitation, and their livers were quickly excised and chilled. Liver was immediately homogenized in 5 volumes of ice-cold polysome buffer containing CHX (100 µg/mL) or LTM (5 µM) using mortar and pestle. Homogenates were centrifuged at 4 °C and 12,000*g* for 10 min, and the supernatant was subjected to puromycin treatment. To dissociate non-initiating ribosomes, cell lysates or liver homogenates were incubated in a solution containing 16 mM HEPES buffer, pH 7.4, 10 mM creatine phosphate, 0.1 mM spermidine, 40 µg/mL creatine phosphokinase, 0.8 mM ATP, and 25 µM puromycin for 15 min. Puromycin-treated samples were then subjected to sucrose gradient sedimentation.

Polysome profiling. Sucrose solutions were prepared in polysome gradient buffer (10 mM HEPES, pH 7.4, 100 mM KCl, 5 mM $MgCl_2$, 100 µg/mL CHX, 5 mM DTT, and 20 U/mL SUPERase_In (Ambion)). Sucrose density gradients (15–45% (wt/vol)) were freshly made in SW41 ultracentrifuge tubes (Fisher) using a BioComp Gradient Master (BioComp) according to the manufacturer's instructions. Puromycin-treated cell lysate was loaded onto sucrose gradients, followed by centrifugation for 100 min at 38,000 r.p.m., 4 °C, in an SW41 rotor. Separated samples were fractionated at 0.375 mL/min by using a fractionation system (Isco) that continually monitored OD_{254} values. Fractions were collected into tubes at 1-min intervals.

Immunoprecipitation of ribosomes from liver polysome fractions. The pooled polysome samples were treated with *Escherichia coli* RNase I (Ambion, 750 U per 100 A260 units) at 4 °C for 1 h to convert the polysome into monosome. Digestion was neutralized with SUPERase inhibitor, and the samples were incubated with 30 µL anti-HA beads (Sigma) at 4 °C overnight. Immunoprecipitates were washed three times with high-salt wash buffer (10 mM HEPES, pH 7.4, 200 mM KCl, 5 mM $MgCl_2$, 1% Nonidet P-40, 1 mM DTT, 100 µg/mL CHX). The washed beads were subjected to RNA extraction for library construction or immunoblotting analysis.

cDNA library construction of ribosome-protected mRNA fragments. To convert the polysome into monosome, we added *E. coli* RNase I (Ambion) into the pooled polysome samples (750 U per 100 A260 units) and incubated at 4 °C for 1 h. SUPERase inhibitor (50 U per 100 U RNase I) was then added to stop digestion. Total RNA extraction was performed using Trizol reagent. Purified RNA samples were dephosphorylated in a 15-µL reaction containing 1× T4 polynucleotide kinase buffer, 10 U SUPERase_In, and 20 U T4 polynucleotide kinase (NEB). Dephosphorylation was carried out for 1 h at 37 °C, and the enzyme was then heat inactivated for 20 min at 65 °C. Dephosphorylated samples were then mixed with 2× Novex TBE-urea sample buffer (Invitrogen) and loaded on a Novex denaturing 15% polyacrylamide TBE-urea gel (Invitrogen). The gel was stained with SYBR Gold (Invitrogen) to visualize the RNA fragments. Gel bands containing RNA species corresponding to 28 nt were excised and physically disrupted by using centrifugation through the holes of the tube. RNA fragments were dissolved by soaking overnight in gel elution buffer (300 mM NaOAc, pH 5.5, 1 mM EDTA, 0.1 U/µL SUPERase_In). The gel debris was removed using a Spin-X column (Corning), and RNA was purified by using ethanol precipitation. Purified RNA fragments were resuspended in 10 mM Tris (pH 8) and denatured briefly at 65 °C for 30 s. Poly(A) tailing reaction was performed in a 8 µL with 1× poly(A) polymerase buffer, 1 mM ATP, 0.75 U/µL SUPERase_ In, and 3 U *E. coli* poly(A) polymerase (NEB). Tailing was carried out for 45 min at 37 °C. For reverse transcription, the following oligos containing barcodes were synthesized: MCA02, 5′-pCAGATCGTCGGACTGTAGAACTCTØCAAGCA GAAGACGGCATACGATT TTTTTTTTTTTTTTTTTTVN-3′; LGT03, 5′-pGTGATCGTCGGACTGTAGAACTCTØCAAGCA GAAGACGGCATACGATT T TTTTTTTTTTTTTTTTTVN-3′; YAG04, 5′-pAGGATCGTCGGACTGTAGAACTCTØCAAGCA GAAGACGGCATACGATT TTTTTTTTTTTTTTTTTTVN-3′; HTC05, 5′-pTCGATCGTCGGACTGTAGAACTCTØCAAGCA GAAGACGGCATACGATT TTTTTTTTTTTTTTTTTTVN-3′, where Ø represents abasic residue.

In brief, the tailed RNA product was mixed with 0.5 mM dNTP and 2.5 mM synthesized primer and incubated at 65 °C for 5 min, followed by incubation on ice for 5 min. The reaction mix was then added with 20 mM Tris (pH 8.4), 50 mM KCl, 5 mM $MgCl_2$, 10 mM DTT, 40 U RNaseOUT, and 200 U SuperScript III (Invitrogen). Reverse transcription reaction was performed according to the manufacturer's instructions. Reverse transcription products were separated on a 10% polyacrylamide TBE-urea gel as described earlier. The extended first-strand product band was expected to be approximately 100 nt, and the corresponding region was excised. The cDNA was recovered by using DNA gel elution buffer (300 mM NaCl, 1 mM EDTA). First-strand cDNA was circularized in 20 µL of reaction containing 1× CircLigase

doi:10.1038/nmeth.3208

buffer, 2.5 mM $MnCl_2$, 1 M betaine, and 100 U CircLigase II (Epicentre). Circularization was performed at 60 °C for 1 h, and the reaction was heat inactivated at 80 °C for 10 min. Circular ssDNA was relinearized with 20 mM Tris-acetate, 50 mM potassium acetate, 10 mM magnesium acetate, 1 mM DTT, and 7.5 U APE 1 (NEB). The reaction was carried out at 37 °C for 1 h. The linearized ssDNA was separated on a Novex 10% polyacrylamide TBE-urea gel (Invitrogen) as described earlier. The expected 100-nt product bands were excised and recovered as described earlier.

Deep sequencing. Single-stranded template was amplified by PCR by using the Phusion high-fidelity (HF) enzyme (NEB) according to the manufacturer's instructions. The oligonucleotide primers qNTI200 (5′-CAAGCAGAAGACGGCATA- 3′) and qNTI201 (5′-AATGATACGGCGACCACCG ACAGGTTCAGAGTTCTAC AGTCCGACG- 3′) were used to create DNA suitable for sequencing, i.e., DNA with Illumina cluster generation sequences on each end and a sequencing primer binding site. The PCR contains 1× HF buffer, 0.2 mM dNTP, 0.5 µM oligonucleotide primers, and 0.5 U Phusion polymerase. PCR was carried out with an initial 30-s denaturation at 98 °C, followed by 12 cycles of 10-s denaturation at 98 °C, 20-s annealing at 60 °C, and 10-s extension at 72 °C. PCR products were separated on a nondenaturing 8% polyacrylamide TBE gel as described earlier. Expected DNA at 120 bp was excised and recovered as described earlier. After quantification by Agilent BioAnalyzer DNA 1000 assay, equal amounts of barcoded samples were pooled into one sample. Approximately 3–5 pM mixed DNA samples were used for cluster generation followed by sequencing by using sequencing primer 5′-CGACAGGTTCAGAGTTC TACAGTCCGACGATC-3′ (Illumina HiSeq).

Preprocessing of ribosome-profiling sequencing reads. Raw ribosome-profiling sequencing reads were first trimmed by 10 nt from the 3′ end, and trimmed reads were further processed by removing adenosine (A) stretches from the 3′ end (one mismatch is allowed). The processed reads between 25 nt and 35 nt were first mapped by TopHat to transcriptome (human: Ensembl release 70; mouse: Ensembl release 66)[32]. The unmapped reads were then mapped to corresponding genome (human: hg19; mouse: mm10). Non-uniquely mapped reads were disregarded for further analysis owing to ambiguity. The 13th position (12-nt offset from the 5′ end) of the uniquely mapped read was defined as the ribosome P-site position. The RPF density was computed after mapping uniquely mapped reads to each individual mRNA transcript according to the NCBI RefSeq gene annotation. For RNA-seq, the raw mRNA sequencing reads (50 nt in length) were mapped to human genome and transcriptome using parameters (--bowtie1 -p 10 -no-novel-juncs). Cuffdiff in the Cufflinks package was used to calculate FPKM values based on Ensembl gene annotation[33].

Prediction of translation initiation sites. Given the fact that many P sites have a small number of GTI-seq reads and the distribution of P-site read count is apparently Poisson overdispersed (unequal mean and variance), we applied zero-truncated binomial negative (ZTNB) model to determine P sites with a statistically significant number of read counts[34]. A global ZTBN model was first fit over all the non-empty P sites of the entire transcriptome. Second, for each individual transcript with more than 50 distinct P-site positions, a local ZTNB model was trained on the nonzero P sites. A putative TIS codon is predicted provided it meets the following criteria: (i) the P site satisfying *P*-value cutoffs (global *P*-value cutoff = 0.05; local *P*-value cutoff = 0.01); (ii) it is a local optimum in a 31-nt window (−15, +15) flanking P-site position; (iii) it is located in the 5′ UTR or in the first one-third of the CDS region. When predicted codons are within 1-nt offset of ATG or near-cognate codon, their coordinates were manually adjusted accordingly.

Quantification of Ribo-seq and QTI-seq. Reads per kilobase per million reads (RPKM) value was calculated to quantify the ribosome occupancy of mRNA for CHX profiling[20]. A window centering the predicted TIS codon (−1, +4) was summarized to represent the abundance of translation initiation signal. To facilitate the comparison between different experimental conditions, we applied upper quartile (UQ) normalization to each predicted TIS codon on the basis of the population of total QTI-seq read count of each individual mRNA[35]. The fold changes of translational signal between two experimental conditions for both LTM and CHX profiling data were normalized by fold changes of RNA-seq FPKM values of the corresponding mRNAs.

Ribosome footprint density aggregation plot. A set of longest mRNA transcripts was compiled by comparing different mRNA isoforms of the same gene on CDS length (if CDS lengths were the same, 5′ UTR lengths were compared). For each ribosome P site in an mRNA, a normalized ribosome density value was calculated by dividing the P-site read count by the average P-site read count across the whole mRNA region (including the CDS and UTRs). Next, all the transcripts were aggregated by averaging each P-site position (relative to start codon or stop codon for the mouse liver data) across all the available transcripts embracing the P-site position.

Volcano plot of aTIS fraction differences. Genes bearing the aTIS and at least another alternative TIS site were retained for drawing volcano plots. The fraction of aTISs among all TISs of a gene was derived by dividing aTIS read count by the sum of read counts of all predicted TISs in the same gene. The difference of aTIS fraction between starvation and control samples was then calculated. To measure the significance of aTIS fraction differences, a permutation test was conducted by randomly redistributing all the TIS reads over predicted TISs. This procedure was repeated 1 million times; each time, the permutated aTIS fraction difference was compared to the aTIS fraction difference in real data at both sides (larger if aTIS fraction difference >0 or smaller if aTIS fraction difference <0). A *P* value was inferred by dividing the number of occurrences where permutated aTIS fraction difference is larger or smaller than the real aTIS fraction differences by the total number of permutations (1 million). The Benjamini-Hochberg algorithm was used to adjust *P* values for estimating false discovery rate (FDR).

Gene Ontology analysis. DAVID was used for gene ontology (GO) enrichment analysis based on PANTHER annotation. The expressed genes (FPKM >1) were used as the background gene set.

Motif analysis. aTISs and uTISs above the change cutoff (twofold change for increased TIS and 0.5-fold change for decreased TIS) after starvation in MEF cell lines were used for motif analysis. A 100-nt sequence flanking the aTIS or uTIS (±50 nt) was retrieved within the context of mRNA. MEME was used to conduct discriminative motif analysis on increased TISs using decreased TISs as the background signal[36]. At each position over the 100-nt flanking sequence of TISs, a motif occurrence frequency was calculated by dividing the number of genes containing enriched motif in the 11-nt window centering current position (±5 nt) by the total number of genes. A scatter plot (*x* axis: relative position to TIS; *y* axis: motif occurrence frequency) was then drawn to reflect the positional distribution of the enriched motif.

Plasmid construction. The 5′ UTRs of interest were amplified by RT-PCR reaction and cloned into pGL3-control vector (Promega). *RPS11*-promoter and *RPS11*-promoter-UTR were amplified from human genome and cloned into pGL3-basic vector (Promega). The sequences of all primers are included in **Supplementary Table 5**.

Luciferase assay. Real-time measurements of Fluc activity were recorded at 37 °C with 5% CO_2 using a Kronos Dio luminometer (Atto) as previously described[37]. In brief, cells were plated on 35-mm dishes and transfected with plasmids encoding Fluc fused with the 5′ UTR of interest. Cells were incubated in HBSS medium for starvation or treated with DOX to induce eIF2α(S51D) expression. 1 mM luciferase substrate d-luciferin (Regis Tech) was added into the culture medium before luminometer measurement.

Immunoblotting. Proteins were resolved on SDS-PAGE and transferred to Immobilon-P membranes (Millipore). Membranes were blocked for 1 h in TBS containing 5% BSA, followed by incubation with primary antibodies at 1:1,000 dilutions. Anti-RPS6 (cat. #2217), anti–phospho-eIF2α (cat. #3398), anti- eIF2α (cat. #5324), anti–phospho-4EBP1 (cat. #9459), and anti-4EBP1 (cat. #9452) antibodies were purchased from Cell Signaling Technology. Anti-RPL5 antibody (SAB1100578) was from Sigma. Anti-HA antibody (SC-7392) was from Santa Cruz Biotechnology. After incubation with horseradish peroxidase–coupled secondary antibodies at 1:1,000 dilutions, immunoblots were developed using enhanced chemiluminescence (ECLPlus, GE Healthcare).

Liver proteasome activity assay. The proteasome chymotrypsin-like activity of liver was detected using Proteasome-Glo chymotrypsin-like Assay kit (Promega) following the manufacturer's instructions. In brief, protein concentration of liver lysates from control mice and fasted mice was measured by Bradford assay. Equal amounts of liver extract were diluted with polysome buffer to a final volume of 100 µL and loaded onto a white 96-well plate. 100 µL of Proteasome-Glu reagent was added to each sample and incubated at room temperature for 10 min. Luminescence was measured by a plate-reading luminometer (BioTek).

***In vitro* translation assay.** Fluc, *Psma3*-Fluc and *Psmb4*-Fluc mRNA were synthesized through *in vitro* transcription using mMessage mMachine T7 Ultra Kit (Ambion). Programmed *in vitro* translation was performed as described previously[38]. A typical reaction contains an equal amount of liver extract, 1× translation buffer (16 mM HEPES, pH 7.6, 10 mM creatine phosphate, 40 µg/mL creatine kinase, 0.1 mM spermidine, 10 µM each amino acid), 80 mM potassium acetate, 1 mM magnesium acetate, 20 U RNase inhibitor (Ambion), 0.8 mM ATP, 0.1 mM GTP and 50 µg/mL mRNA template. *In vitro* translation reactions were incubated at 37 °C for 2 h, and luciferase activity was measured with luciferase substrate (Promega).

Code availability. All the procedures but sequencing mapping were completed using custom R or Python scripts. These scripts are available upon request.

32. Trapnell, C., Pachter, L. & Salzberg, S.L. TopHat: discovering splice junctions with RNA-Seq. *Bioinformatics* **25**, 1105–1111 (2009).
33. Trapnell, C. *et al.* Transcript assembly and quantification by RNA-Seq reveals unannotated transcripts and isoform switching during cell differentiation. *Nat. Biotechnol.* **28**, 511–515 (2010).
34. Hilbe, J.M. *Negative Binomial Regression* 2nd edn. (Cambridge Univ. Press, 2011).
35. Dillies, M.A. *et al.* A comprehensive evaluation of normalization methods for Illumina high-throughput RNA sequencing data analysis. *Brief. Bioinform.* **14**, 671–683 (2013).
36. Bailey, T.L. *et al.* MEME Suite: tools for motif discovery and searching. *Nucleic Acids Res.* **37**, W202–W208 (2009).
37. Sun, J., Conn, C.S., Han, Y., Yeung, V. & Qian, S.B. PI3K-mTORC1 attenuates stress response by inhibiting cap-independent Hsp70 translation. *J. Biol. Chem.* **286**, 6791–6800 (2011).
38. Liu, B., Han, Y. & Qian, S.B. Cotranslational response to proteotoxic stress by elongation pausing of ribosomes. *Mol. Cell* **49**, 453–463 (2013).

doi:10.1038/nmeth.3208